


Characterization and Quantification of Image Quality in CT Imaging Systems: A Phantom Study

Camilla Scapicchio^{1,2} ^a, Manuela Imbriani^{1,3}, Francesca Lizzi², Mariagrazia Quattrocchi³,
Alessandra Retico², Sara Saponaro^{1,2}, Maria Irene Tenerani^{1,2}, Alessandro Tofani³,
Arman Zafaranchi^{1,2} and Maria Evelina Fantacci^{1,2}

¹University of Pisa, Pisa, Italy

²National Institute for Nuclear Physics, Pisa, Italy

³Medical Physics Department, Azienda Toscana Nord Ovest Area Nord, Lucca, Italy

Keywords: Computed Tomography, Image Quality, Detectability Index, CatPhan Phantom.


Abstract: Computed Tomography (CT) is a widely used imaging technique in lung cancer screening programs. To address the problem of exposing potentially healthy patients to ionizing radiation, Iterative Reconstruction (IR) algorithms can be employed. Indeed, traditional Filtered Back Projection reconstruction does not deliver adequate image quality with reduced dose levels. IR instead is prone to preserve diagnostic information and resolution while reducing noise and radiation dose. We characterized image quality for two CT scanners equipped with different iterative algorithms by using a quantitative metric, the detectability index. We compared the dependence of the image quality on the dose and the iterative level when the human visual perception is considered or not in the detectability index definition. It has been found that similar image quality can be obtained by using different scanners and different combinations of dose and iterative levels. This allows us to extrapolate the protocols corresponding to a lower dose while preserving as much as possible the imaging properties.

1 INTRODUCTION

Chest Computed Tomography (CT) is the best and most used imaging modality to detect small pulmonary nodules that are the early radiological signs of lung cancer (Raju et al., 2017; Kennedy et al., 2022). It is recommended as a screening tool in high-risk populations, thus exposing potentially healthy people to ionizing radiation (Yeh et al., 2016; Cao et al., 2022). For this reason, in recent years a wide effort has been dedicated to the development of new strategies to reduce the radiation dose delivered to the patient during the CT acquisition complying with the ALARA principle (radiation doses should be kept As Low As Reasonably Achievable) while maintaining the same imaging properties (Smith-Bindman et al., 2019). In particular, the advent of Iterative Reconstruction (IR) algorithms has been one of the main advances in CT technology introduced to reduce the image noise in diagnostic images (Beister et al., 2012; Caramella et al., 2018), thereby allowing for the re-

duction of the dose required for routine imaging. However, the use of IR algorithms is limited by the necessity of preserving the image quality to capture diagnostic information. The intrinsic non-linear nature of the IR reconstruction algorithms compared to conventional Filtered Back-Projection (FBP) has been highlighted (Dodge et al., 2016). Therefore the traditional metrics, such as the Contrast-To-Noise ratio or the Modulation Transfer Function (MTF), appear to be inadequate to comprehensively describe clinical imaging performance when IR techniques are used for image reconstruction (Samei et al., 2019). This is because IR algorithms result in object-dependent resolution and noise performances. An accurate evaluation and optimization of the best IR blending levels for the different possible applications is needed to define new low-dose diagnostic protocols (Barca et al., 2018a).

Nowadays powerful instruments based on Artificial Intelligence (AI) have also been developed to extract significant diagnostic information from chest CT images acquired with a lower radiation dose. This offers new perspectives on lung cancer diagnosis and

^a  <https://orcid.org/0000-0001-5984-0408>

other lung pathologies. However, a more specific analysis of image quality has to be implemented when the CT scans are aimed to be provided to an AI algorithm.

In this study, we characterize two CT scanners in terms of image quality across different acquisition and reconstruction parameters by means of phantom image acquisitions. It is not so easy to define a comprehensive metric that quantifies image quality, because different objective measures can impact it, such as resolution, noise, and contrast. Typically it is useful to consider these measures separately. However, for some applications, it is useful to have a unique definition to quantify image quality as a whole. We adopted a new comprehensive more adequate metric to quantitatively define the image quality, which is the detectability index (d') (Samei et al., 2019). It allows us to evaluate the joint effect of all the factors that can impact image quality. This new index is also more suitable to describe image quality when IR algorithms are used.

The main objective of this study is to evaluate the imaging properties of chest CT reconstructed with different Iterative Reconstruction blending levels by leveraging this new detectability index in order to find a strategy to reduce the radiation dose delivered in CT acquisitions without degrading the imaging properties. The possibility of using IR algorithms in conjunction with CAD (Computer Aided Detection) systems has already been investigated as useful to bring an improvement in image quality when very low radiation exposure levels are employed (Caramella et al., 2018; Barca et al., 2018b). In addition, nowadays these CAD systems are being updated with new Deep Learning-based tools (Manickavasagam et al., 2022; Forte et al., 2022). Thus the image quality characterization here proposed is finally aimed at applying Deep Learning- or Radiomics-based image analysis systems.

2 MATERIALS

2.1 Phantom and CT Scanners

The phantom under consideration is the model Catphan-500 © (The Phantom Laboratory, NY, USA). It is a commercially available phantom commonly utilized in clinical procedures for quality control aimed at ensuring ideal imaging performance for a CT scanner. It has a cylindrical shape and it is composed of 4 modules (Figure 1). Full technical specifications of the Catphan-500 phantom can be found in the manual (Mail, 2013).

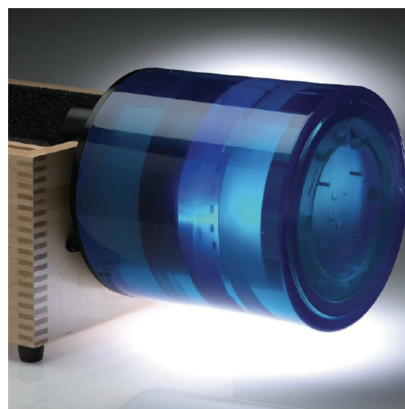


Figure 1: Illustration of the Catphan-500 phantom model (Mail, 2013).

In this study, the CTP401 and CTP486 modules of the phantom were considered for the computation of the detectability index. The CTP486 module is a homogeneous water-equivalent module. The CTP401 module includes seven cylindrical inserts of different materials, with the nominal CT Hounsfield Units (HU) reported in the manual (Mail, 2013), in a uniform water-equivalent background.

The CT scans of the Catphan phantom have been acquired at San Luca Hospital-Azienda Toscana Nord Ovest (ATNO)-Lucca, Italy. We used the two CT scanners from two different vendors available in this hospital: Revolution Evo 64 Slice (GE Healthcare), and Aquilon CX 128 Slice CT (Toshiba).

2.2 Image Data Acquisition

The phantom was scanned in helical modality. We aimed to characterize image quality in conditions as close as possible to those of lung imaging. Therefore, we started from the institutional clinical CT protocols for diagnostic tasks in chest imaging used in the Hospital for the two scanners ($CTDI_{vol} \sim 7mGy$ for the GE scanner, and $CTDI_{vol} \sim 8mGy$ for the Toshiba scanner). Then we explored three other dose radiation levels: high (twice the standard value, i.e. the one of the institutional protocol), reduced (60% of the standard value), and low (30% of the standard value). We also used four percentages of the IR blending level (FBP alone and three increasing strength levels of the IR algorithm available for the system, which is the ASIR for GE and the ADR 3D for Toshiba). A sharp reconstruction kernel has been used in both systems: LUNG for GE, and FC56 (equivalent to LUNG) for Toshiba. The complete list of parameters set in the two scanners is reported in Table 1. Each acquisition with the same set of parameters has been repeated 3 times, each time removing and repositioning the

phantom. A total of 96 CT scans of the phantom were made available at the end of the acquisition process.

3 METHODS

3.1 Image Quality Quantification

The new comprehensive more adequate task-based metric that we used to quantify image quality is the detectability index d' . It is based on model observer methodologies that try to combine the system image performance, the task characteristics, and the degree of clinician image perception (Vennart, 1997). The procedure to compute the detectability index is reported in the American Association of Physicists in Medicine task group report-23 (AAPM TG-233) (Samei et al., 2019). We adopted the d' definition presented in this report:

$$d'^2 = \frac{\left[\int \int |W|^2 TTF^2 E^2 dudv \right]^2}{\int \int |W|^2 TTF^2 NPS^2 E^2 dudv} \quad (1)$$

where W is the Task function, i.e., the Fourier transform of a synthesized ideal image of a signal to be detected. In fact, the d' index quantifies the degree of separation for signal present/signal absent distributions on the image. We considered a signal with a circular shape and a designer contrast profile. The TTF is the Task Transfer Function that is a representative metric of spatial resolution. It replaces the traditional MTF that may not represent the imaging system's response to an arbitrary input object because the system resolution becomes dependent on the object contrast and background noise level. Instead, when reporting TTF , the background noise, the object's contrast, and the object's radial location are included. This is the reason why d' is more suitable when IR algorithms are used. NPS is the Noise Power Spectrum that summarizes the noise texture in the spatial frequency domain. E is a function that simulates the eye filter modeling the human visual system sensitivity to different spatial frequencies. The arrays should have the same shape, typically representing frequency values along the u and v dimensions.

Hence, the detectability index, depending on spatial resolution, contrast and noise, in turn, depends on the dose, tube potential, tube current modulation setting, phantom size, task size, task contrast, image thickness, reconstruction algorithm, and reconstruction kernel. It is therefore evident that this metric allows us to evaluate the joint effect of all the factors that can impact image quality.

To compute the detectability index on our phantom CT images with a semi-automatic procedure, we used the *imQuest* open-source software (Duke University, Durham, NC, USA) (Solomon, 2018). Once each CT scan is uploaded, the *imQuest* software requires the first step of TTF computation (Figure 2). An insert has to be chosen as a reference and we placed a circular ROI with a radius about twice that of the chosen insert (~ 60 pixels) on it. In this manuscript, we will show the results related to polystyrene (with a nominal object-to-background contrast ($|\Delta HU| \approx 100$) adequate for low-contrast diagnostic tasks) and air inserts. However, we repeated the d' computation by also considering all the other inserts. The second step is the NPS computation. Five 64×64 pixels ROIs in the CTP486 homogenous module (Figure 2) have been drawn. The $2D-NPS$ is then computed as the area-normalized Fourier transform of the ROI.

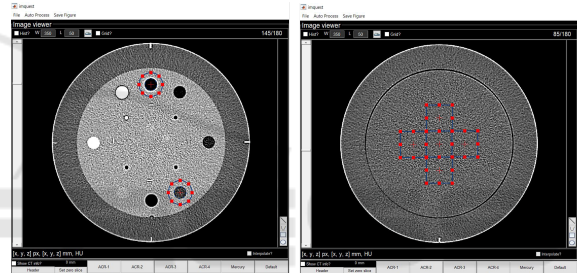


Figure 2: Manually ROI placement for TTF (on the left) and NPS (on the right) computation on *imQuest*.

Then, the W parameters have to be set in *imQuest*. We wanted to simulate a 5-mm diameter lesion with the contrast automatically taken from the insert considered for the TTF computation. Therefore the parameters set in *imQuest* were: designer contrast profile, signal diameter of 5 mm, profile exponent of 1. For the eye filter E , we used the NPWE model observer obtained with the non-prewhitening matched filter by adding the eye filter correction (Burgess, 1994), selecting the radial noise generation mode and the Saunders visual response function. To reproduce the working scenario of radiologists, we also set the following interpretation conditions: display pixel pitch of 0.2 mm, zoom factor of 1.74, viewing distance of 500 mm, and a field of view of 380 mm. Once all these steps are performed, the software automatically outputs the detectability index value, by using the equation (1).

Table 1: Acquisition and reconstruction parameters used for the two scanners. The $CTDI_{vol}$ is the weighted average measurement of the dose in a reference phantom, expressed in mGy .

	REVOLUTION GE	AQUILON TOSHIBA
$CTDI_{vol}$ [mGy] (Tube current [mA])		
High	13.52 (160)	16.50 (300)
Standard	6.76 (80)	8.30 (150)
Reduced	4.06 (50)	5.00 (90)
Low	2.03 (25)	2.49 (45)
DATA ACQUISITION		
Tube potential (kVp)	120	120
Pitch	0.984	0.938
IMAGE RECONSTRUCTION		
Display field of view (mm)	210	219
Pixel Spacing (mm)	0.406	0.427
Slice thickness (mm)	1.25	1.00
Kernel	LUNG	FC56
Reconstruction algorithm	FBP, ASIR	FBP, AIDR 3D
Iterative level	0%, 10%, 40%, 70%	0%, mild, standard, strong

3.2 Characterization of CT Protocols in Terms of Image Quality

In order to characterize the CT protocols in terms of image quality, we first plotted the mean detectability index value, computed on the three identical acquisitions, as a function of the $CTDI_{vol}$, highlighting the different combinations of the changed parameters (scanner, dose level, and IR blending level). Then we also visualized how the d' , i.e., image quality varies with the $CTDI_{vol}$ alone and, by means of a color map, how it varies simultaneously with the $CTDI_{vol}$ and the IR level, for each scanner separately.

3.3 Image Quality with and Without the Eye Filter

To make the d' computation more automatic and have full control over each step, we have also developed a Python script that takes as input the CT image, the coordinate of the center and the radius of the ROIs for the TTF computation and automatically returns the detectability index value, besides the 2D TTF and the 2D NPS. The Python code will be made available after the study is completed. Since there is no available documentation on the mathematical form of the eye filters available in imQuest, we adopted the following definition (Solomon et al., 2015):

$$E(\rho) = |\eta\rho^{1.5} \cdot e^{-0.98 \cdot \rho^{0.68}}|^2 \quad (2)$$

We computed the d' values for the images acquired on the phantom also with this automated program, obtaining the d'_{NPE} with the previous equation (1), but considering this definition of the eye filter.

However, it is also possible to define the detectability index without the addition of the eye filter, with the definition 3. In this case, we quantify a sort of "objective" image quality not related to the human vision perception.

$$d'_{NPW}{}^2 = \frac{\left[\int \int |W|^2 TTF^2 dudv \right]^2}{\int \int |W|^2 TTF^2 NPS^2 dudv} \quad (3)$$

We leveraged the automated code to re-compute this detectability index without adding the eye filter.

We finally compared the dependence of d' on the acquisition/reconstruction parameters in the two cases, when image quality comprises how the image appears to the human visual system and when it is not based on visual perception.

4 RESULTS

In Figure 3, the plots of the mean detectability index value, computed on the three identical acquisitions, referred to both the polystyrene and air inserts, as a function of the $CTDI_{vol}$ are shown. However, the three parameters that we changed in the acquisition/reconstruction phase, scanner, $CTDI_{vol}$ and iterative blending level, were highlighted for each point.

As evident from the plots, the range assumed by the d' value varies. This was expected given the different contrast of the two inserts. It is also possible to identify in the plots different protocols, i.e., different combinations of scanner-dose-iterative level parameters that produce a similar value of the detectabil-

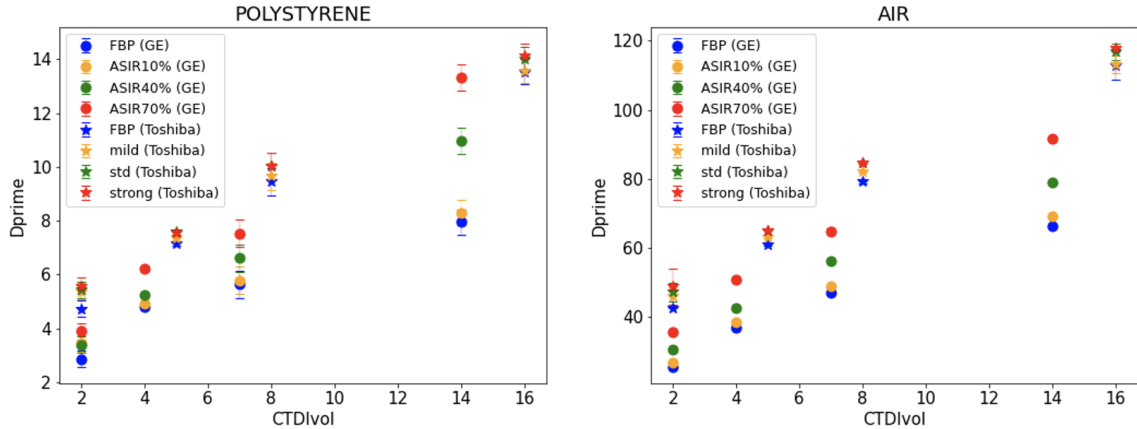


Figure 3: Plots of the mean detectability index as a function of the $CTDI_{vol}$ for both the polystyrene and air inserts. The circles are used for the GE scanner and the stars for the Toshiba scanner. In the legend, the colors are corresponding to the iterative levels for the two scanners.

Table 2: Set of acquisition/reconstruction parameters corresponding to the protocols providing a similar detectability index. STD:STANDARD.

Scanner	$CTDI_{vol}$	Iterative level
GE	4	ASIR 70%
GE	7	ASIR 0%
GE	7	ASIR 10%
GE	7	ASIR 40%
GE	7	ASIR 70%
GE	14	ASIR 0%
GE	14	ASIR 10%
Toshiba	2	AIDR3D MILD
Toshiba	2	AIDR3D STD
Toshiba	2	AIDR3D STRONG
Toshiba	5	FBP
Toshiba	5	AIDR3D MILD
Toshiba	5	AIDR3D STD
Toshiba	5	AIDR3D STRONG

ity index, meaning that they produce a similar image quality. This was equally observed for the d' from the other five inserts in the CTP401 module of the phantom. Hence this observation is not restricted to a specific insert or material, but having a similar trend, it is generalizable to all inserts under examination. It is interesting to observe that these "equivalent" protocols reported in Table 2 are heterogeneous in terms of scanner, $CTDI_{vol}$ and iterative levels.

We visually inspected the images obtained with protocols that produce a similar d' and we compared them to images obtained with protocols that produce a very different d' , always extrapolated from the plots in Figure 3. It was observed that a similarity in image appearance can be perceived for the protocols corresponding to a similar detectability index. Instead,

when we inspect images obtained with protocols producing a different d' , they present a quite different appearance, especially in terms of noise. Therefore, the detectability index could be a reasonable index to "quantify" image quality.

As for the plot of d' as a function of the dose alone and the colormaps of d' as a function of both dose and iterative level, they are represented for the polystyrene insert in Figure 4, for both GE and Toshiba scanners.

In Figure 5, the same plot of Figure 3 for the polystyrene insert is represented, with the difference that the d' value has been obtained with the automated program, and thus by using the eye filter defined in (2). Therefore, the trend is the same but the range of values assumed by d' is different (also because the lesion diameter simulated for the task function W was set to 12 mm in the script and is different from the one of 5 mm set on imQuest). It can be compared to the plot obtained for the detectability index as defined by equation (3), namely without considering the eye filter, shown in Figure 6.

From these two graphs, it can be observed that in both cases, the dependence of d' on the protocol is similar. Also, in these cases, some protocols that produce a similar detectability index and thus a similar image quality can be identified. However, when we do not consider the eye filter it is evident that by increasing the iterative level, there is not an evident improvement in image quality as in the case in which we consider the eye filter. This is particularly true for the ASIR algorithm in the GE scanner. It seems that when we do not evaluate the quality based on visual perception, the image quality at lower doses continues to improve as ASIR increases. Still, it appears to worsen at higher doses.

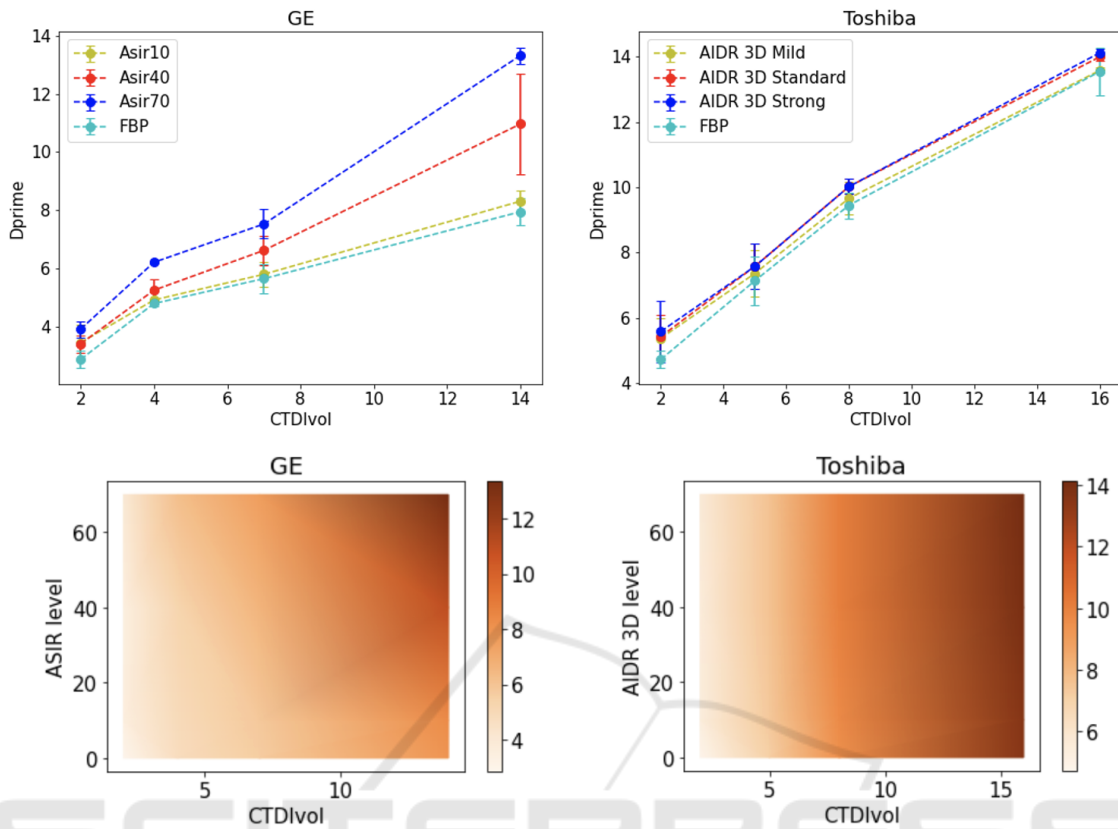


Figure 4: Upper row: Mean detectability index of polystyrene insert as a function of the dose level. Lower row: color maps of the mean detectability index of polystyrene insert as a function of both dose level and iterative level. The color intensity corresponds to the d' value.

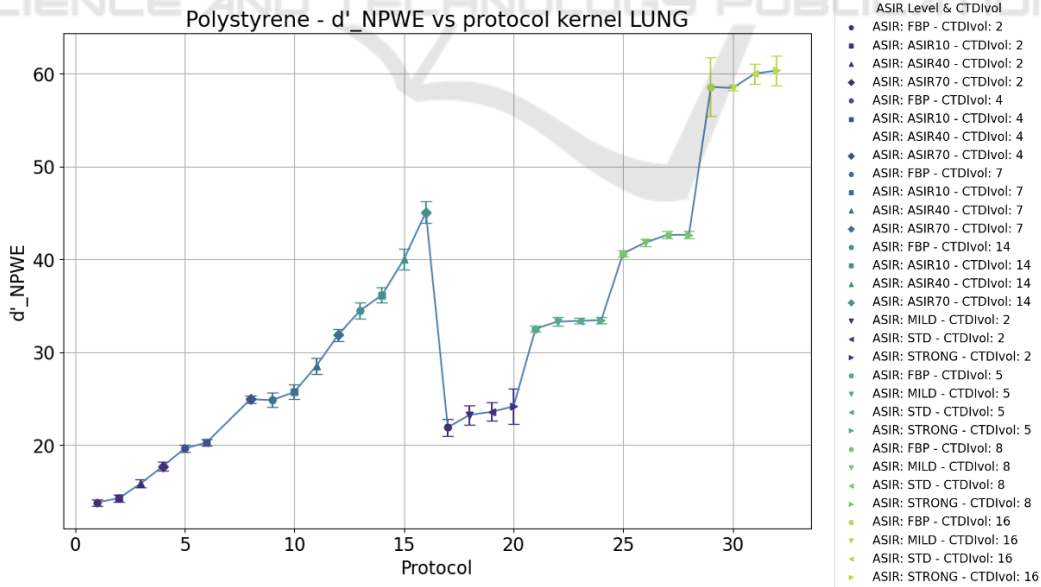


Figure 5: Plot of the mean detectability index as a function of the protocol for polystyrene. d' values are output from the Python script by using the definition in 1 and the expression 2 for the eye filter.

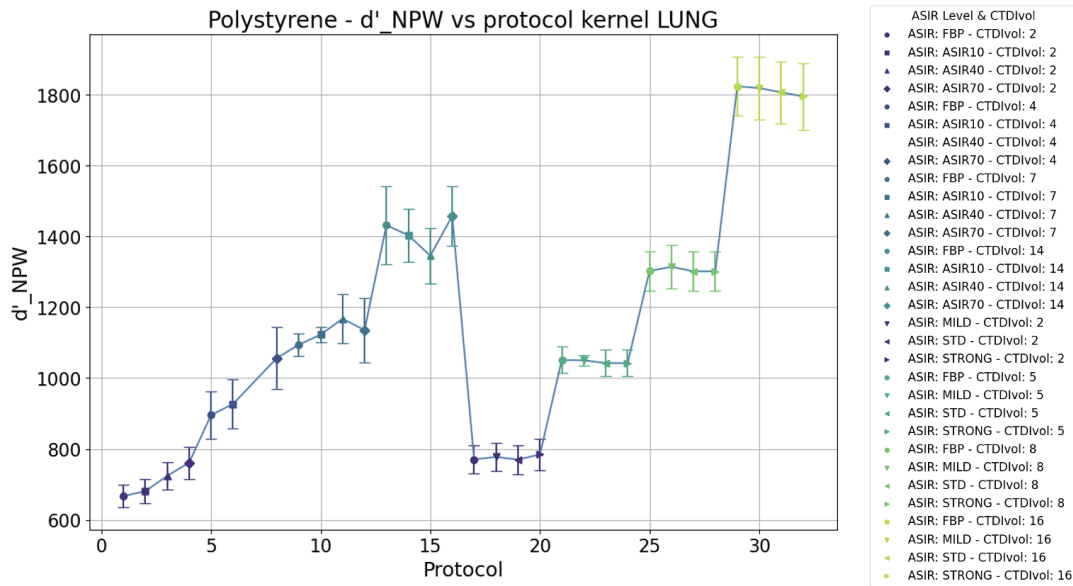


Figure 6: Plot of the mean detectability index as a function of the protocol for polystyrene. d' values are output from the Python script by using the definition in 3 without the eye filter.

5 DISCUSSION

In this study, we characterized two CT scanners in terms of image quality, which was quantified by means of a new metric, the detectability index, more suitable for images with iterative algorithm reconstruction. We found that it is possible to identify “equivalent” protocols, meaning protocols that produce a similar d' , i.e., a similar image quality. From these “equivalent” protocols, it would be possible to extrapolate those that correspond to a lower dose level. In other words, it is possible to find the optimal protocol to reduce the radiation dose delivered in CT acquisitions without degrading the imaging properties. These results confirm the ones obtained in another similar study (Muti et al., 2023).

The conclusions of our study also pave the way for new perspectives in radiomics study. We have indeed started to analyze if these “equivalent” protocols can be leveraged to obtain more robust extracted radiomics features, in order to define a new possible harmonization strategy based on matching image quality. The analysis on using or not the eye filter while evaluating image quality poses another important question. In fact, the obtained results demonstrate that a further exploration of the iterative algorithms effect is needed. We hypothesized that the worsening of image quality at higher iterative levels while maintaining the dose constant could be related to the blurring that ASIR causes in the image. However, this should be further investigated. The interesting note

is that increasing the iterative level of some iterative algorithms like ASIR can improve the image quality as it is perceived by human eyes. Still, it can determine a worsening when we consider a more ‘objective’ quality not related to the human visual system. This should be further investigated when the images have to be finally provided to an AI algorithm, which is naturally not equipped with a visual filter.

A possible limitation to the analysis presented in this paper is that d' is a task-based image quality metric, therefore it depends on the specific task function chosen to represent a task in clinical practice. We simulated a 5-mm diameter lesion with a specific contrast but this is not the only one that could be considered.

Moreover, this study is preliminary as in order to claim the consistency of our results the analysis should be extended to other clinical centers and scanners, possibly equipped with different types of iterative algorithms, and exploring other protocols and a wider range of parameters. Therefore, the future perspectives are in parallel refining the analysis by introducing more variables and investigating a possible harmonization strategy based on this characterization of image quality to improve the robustness of radiomics studies.

ACKNOWLEDGEMENTS

This research has been developed as part of a Ph.D. program in collaboration with the University of Pisa and the National Institute for Nuclear Physics (INFN). Research partly supported by: Artificial Intelligence in Medicine (next_AIM, <https://www.pi.infn.it/aim>) project, funded by INFN-CSN5; FAIR-AIM project funded by Tuscany Government (POR FSE 2014-2020); PNRR - M4C2 - Partenariato Esteso "FAIR - Future Artificial Intelligence Research" - Spoke 8, and PNRR - M4C2 - Centro Nazionale "ICSC - Centro Nazionale di Ricerca in High Performance Computing, Big Data and Quantum Computing" - Spoke 8, funded by the European Commission under the NextGeneration EU programme; the Italian Ministry of Health Grant RC and 5x1000 Health Research; AIMS2-Trials, <http://aims-2-trials.eu>; the European Union NextGenerationEU through the Italian Ministry of University and Research under PNRR M4C2-I1.3 Project PE_00000019 "HEAL ITALIA" to Maria Evelina Fantacci and Arman Zafaranchi CUP I53C22001440006. The views and opinions expressed are those of the authors only and do not necessarily reflect those of the European Union or the European Commission Neither the European Union nor the European Commission can be held responsible for them.

REFERENCES

- Barca, P., Giannelli, M., Fantacci, M. E., and Caramella, D. (2018a). Computed tomography imaging with the adaptive statistical iterative reconstruction (asir) algorithm: dependence of image quality on the blending level of reconstruction. *Australasian physical & engineering sciences in medicine*, 41:463–473.
- Barca, P., Palmas, F., Fantacci, M. E., and Caramella, D. (2018b). Evaluation of the adaptive statistical iterative reconstruction algorithm in chest ct (computed tomography).
- Beister, M., Kolditz, D., and Kalender, W. A. (2012). Iterative reconstruction methods in x-ray ct. *Physica medica*, 28(2):94–108.
- Burgess, A. (1994). Statistically defined backgrounds: performance of a modified nonprewhitening observer model. *JOSA A*, 11(4):1237–1242.
- Cao, C.-F., Ma, K.-L., Shan, H., Liu, T.-F., Zhao, S.-Q., Wan, Y., and Wang, H.-Q. (2022). Ct scans and cancer risks: A systematic review and dose-response meta-analysis. *BMC cancer*, 22(1):1238.
- Caramella, D., Fantacci, M. E., Palmas, F., Barca, P., et al. (2018). Evaluation of the adaptive statistical iterative reconstruction algorithm in chest ct (computed tomography)-a preliminary study toward its employment in low dose applications, also in conjunction with cad (computer aided detection). In *Proceedings of the 11th International Joint Conference on Biomedical Engineering Systems and Technologies-Volume 5: AI4Health*, volume 5, pages 688–694.
- Dodge, C. T., Tamm, E. P., Cody, D. D., Liu, X., Jensen, C. T., Wei, W., Kundra, V., and Rong, X. J. (2016). Performance evaluation of iterative reconstruction algorithms for achieving ct radiation dose reduction—a phantom study. *Journal of applied clinical medical physics*, 17(2):511–531.
- Forte, G. C., Altmayer, S., Silva, R. F., Stefani, M. T., Libermann, L. L., Cavion, C. C., Youssef, A., Forghani, R., King, J., Mohamed, T.-L., et al. (2022). Deep learning algorithms for diagnosis of lung cancer: a systematic review and meta-analysis. *Cancers*, 14(16):3856.
- Kennedy, K., Hulbert, A., Pasquinelli, M., and Feldman, L. E. (2022). Impact of ct screening in lung cancer: Scientific evidence and literature review. In *Seminars in Oncology*. Elsevier.
- Mail, T. B. (2013). Catphan® 500 and 600 m anual. *The Phantom Laboratory*.
- Manickavasagam, R., Selvan, S., and Selvan, M. (2022). Cad system for lung nodule detection using deep learning with cnn. *Medical & Biological Engineering & Computing*, 60(1):221–228.
- Muti, G., Riga, S., Berta, L., Curto, D., De Mattia, C., Felisi, M., Rizzetto, F., Torresin, A., Vanzulli, A., and Colombo, P. E. (2023). Performance of three model-based iterative reconstruction algorithms using a ct task-based image quality metric. *arXiv preprint arXiv:2301.08691*.
- Raju, S., Ghosh, S., and Mehta, A. C. (2017). Chest ct signs in pulmonary disease: a pictorial review. *Chest*, 151(6):1356–1374.
- Samei, E., Bakalyar, D., Boedeker, K. L., Brady, S., Fan, J., Leng, S., Myers, K. J., Popescu, L. M., Ramirez Giraldo, J. C., Ranallo, F., et al. (2019). Performance evaluation of computed tomography systems: summary of aapm task group 233. *Medical physics*, 46(11):e735–e756.
- Smith-Bindman, R., Wang, Y., Chu, P., Chung, R., Einstein, A. J., Balcombe, J., Cocker, M., Das, M., Delman, B. N., Flynn, M., et al. (2019). International variation in radiation dose for computed tomography examinations: prospective cohort study. *Bmj*, 364.
- Solomon, J., Wilson, J., and Samei, E. (2015). Characteristic image quality of a third generation dual-source mdct scanner: noise, resolution, and detectability. *Medical physics*, 42(8):4941–4953.
- Solomon, J. B. (2018). Performance evaluation of computed tomography systems. resources: Aapm tg-233.
- Vennart, W. (1997). Icru report 54: Medical imaging-the assessment of image quality-isbn 0-913394-53-x. april 1996, maryland, usa. *Radiography*, 3(3):243–244.
- Yeh, D.-M., Tsai, H.-Y., Tyan, Y.-S., Chang, Y.-C., Pan, L.-K., and Chen, T.-R. (2016). The population effective dose of medical computed tomography examinations in taiwan for 2013. *PLoS One*, 11(10):e0165526.